

VIBRATIONALLY EXCITED MOLECULAR HYDROGEN NEAR HERSCHEL 36

BRIAN L. RACHFORD

Department of Physics, Embry-Riddle Aeronautical University, 3700 Willow Creek Road, Prescott, AZ 86301-3720; rachf7ac@erau.edu

THEODORE P. SNOW

Center for Astrophysics and Space Astronomy, Department of Astrophysical and Planetary Sciences, University of Colorado, Boulder, CO 80309-0389

TERESA L. ROSS

Department of Astronomy, New Mexico State University, Las Cruces, NM 88003-8001

Draft version April 8, 2014

ABSTRACT

We present the first high resolution UV spectra toward Herschel 36, a Trapezium-like system of high-mass stars contained within the Lagoon Nebula (M8, NGC 6523). The spectra reveal extreme ro-vibrational excitation of molecular hydrogen in material at a single velocity or very small range of velocities, with this component presumably lying near the star system and undergoing fluorescent excitation. The overall H₂ excitation is similar to, but apparently larger than, that seen towards HD 37903 which previously showed the largest vibrationally excited H₂ column densities seen in UV absorption spectra. While the velocities of the highly excited H₂ lines are consistent within each observation, it appears that they underwent a ~ 60 km s⁻¹ redshift during the 3.6 years between observations. In neither case does the velocity of the highly excited material match the velocity of the bulk of the line-of-sight material which appears to mostly be in the foreground of M8. Recent work shows unusually excited CH and CH⁺ lines and several unusually broad Diffuse Interstellar Bands towards Herschel 36. Along with the H₂ excitation, all of these findings appear to be related to the extreme environment within ~ 0.1 pc of the massive young stellar system.

Subject headings: ISM: abundances — ISM: clouds — ISM: lines and bands — ISM: molecules — ultraviolet: ISM

1. INTRODUCTION

The Lagoon Nebula (M8, NGC 6523) is one of the most prominent bright nebulae in the sky, and contains regions of recent star formation and many early-type stars. The optically brightest portion of the nebula lies near the object Herschel 36¹. Previously considered a single O-type star, Herschel 36 has recently been spectroscopically resolved into a O7.5 V star in a ~ 500 -day, ~ 3 au mutual orbit with a close late-O/early-B binary (Arias et al. 2010). The presence of an additional heavily embedded star of early B-type has been inferred 0.25 arcsec (375 au at 1500 pc) southeast of the triplet (Goto et al. 2006). The Herschel 36 system thus has much in common with the Trapezium system in the Orion Nebula.

The hot stars, presumably dominated by the O7.5 V component, are the primary illuminating source for the bright region 15" east of Herschel 36, known as the Hourglass for its distinctive shape in optical images (Thackeray 1950, Wolff 1961). Additional hot stars ionize the extended H II region surrounding the Hourglass. Infrared radiation from the embedded early B-type star may be responsible for the unusually high excitation of CH and CH⁺ seen in optical spectra towards Herschel 36 (Oka et

al. 2013).

The Herschel 36 system is highly obscured by dust ($E(B-V) = 0.87$), and the line of sight shows exceptional extinction characteristics. The total-to-selective extinction ratio, $R_V \equiv A_V/E(B-V) = 5.21 \pm 0.10$ (Fitzpatrick & Massa 2007), is one of the largest known and a correction for foreground material suggests an even larger R_V for material local to Herschel 36 (Hecht et al. 1982). This value is consistent with a population of larger than normal dust grains. The far-UV extinction curve is correspondingly shallow (Fitzpatrick & Massa 2007), and it is the very weak UV extinction that allows sufficient transmission of light for far-UV observations.

While the Hourglass and the general region around Herschel 36 have been studied extensively at various wavelengths (see Dahlstrom et al. 2013 for a review) there has been no previous UV spectroscopy toward Herschel 36 with sufficient resolution and S/N for interstellar absorption line studies. In this paper, we give the results of such an investigation, focusing on the highly unusual molecular hydrogen absorption seen along the line of sight.

2. OVERVIEW OF THE DATA

2.1. Observations

Herschel 36 was observed twice by the *Far Ultraviolet Spectroscopic Explorer (FUSE)* as part of the PI Team “translucent” cloud program (Rachford et al. 2002); see Table 1 for observation details. Although our initial anal-

¹ This star is sometimes associated with the designation HD 164740, but the relevant entry in the Henry Draper catalog (Cannon & Pickering 1922) indicates that object 164740 is nebular. This is presumably the bright Hourglass region described in the next paragraph, and not the star described by J. Herschel (1847), which has the identifier CD -24 13806.

TABLE 1
FUSE OBSERVATIONS

| Data Set ID | Date | Exp. time (ksec) | Aperture |
|-------------|-------------|---------------------|----------|
| P1162001 | 2000 Aug 30 | 10.6 | LWRS |
| P1162002 | 2004 Apr 8 | 5.9 | LWRS |

ysis involved earlier data products, for our final results we used data downloaded from the Mikulski Archive for Space Telescopes (MAST) in late 2011, which was processed with version 3.2.1 of the CALFUSE pipeline. While data are present shortward of 1000 Å down to near the Lyman limit, the S/N is quite poor at these wavelengths. Thus, we have focused on data longward of 1000 Å in the LiF 1A channel (987.4–1082.7 Å) and the LiF 2A channel (1086.9–1181.5 Å) (see Moos et al. 2000 for more information on the configuration of the *FUSE* spectrograph). The velocity resolution is $\Delta v \approx 15$ –20 km/s, depending on wavelength and instrument channel. Outside of the deep absorption bands of H₂ and other strong absorption features, the S/N per resolution element is typically 15–30 with the best S/N occurring at wavelengths longer than 1100 Å.

2.2. The H₂ spectrum

The overall far-UV spectrum is typical of significantly reddened stars, as it is dominated by absorption from H I and H₂, the latter in the form of damped ro-vibrational bandheads due to absorption from the $J = 0$ and $J = 1$ levels.² However, a closer look at the spectra reveals three unusual features.

First, we see a large number of weak lines corresponding to absorption from excited vibrational states. A sample of these lines is given in Figure 1. Vibrational excitation of H₂ in diffuse and translucent lines of sight of sufficient magnitude to be detected with *FUSE* is quite rare. Prominent examples include the lines of sight toward HD 34078 (Boissé et al. 2005), and HD 37903 (Gnaniński 2011). Only the latter is comparable with the Herschel 36 spectrum in terms of the quantity and strength of vibrationally excited lines. Second, when looking at lines from the $J = 2$ –4 levels of the ground vibrational state, we see a broad velocity structure spread across tens of km s^{−1}. Finally, we see a significant velocity shift in a portion — but not all — of the material between the first observation and the second.

The highly excited material is a compelling issue on its own; in fact it appears to be the strongest such excitation seen to date in ultraviolet absorption spectra. Recent work has also revealed unusually strong excitation of the CH and CH⁺ molecules along this line of sight, as well as extended redward wings in several Diffuse Interstellar Bands (DIBs) consistent with excitation of higher than normal rotational states in the molecules that presumably produce the DIB absorption (Dahlstrom et al. 2013).

A full understanding of the velocity structure and changes in velocity structure seen in the *FUSE* spectra

will likely require additional data and analysis. However, considerable information on excited H₂ is available from just the existing *FUSE* spectra. Thus, in this paper we will mainly focus on the excited H₂ and explore the other two issues only as they directly relate to the highly excited material.

3. ANALYSIS AND INTERPRETATION

3.1. Line measurements and curve-of-growth analysis

The lines from $J \geq 5$ of the ground vibrational state, and lines from the excited vibrational states are narrow enough to be consistent with the resolution of the spectrograph. Thus, any velocity structure is buried within the resolution element, and we will treat those lines as representing a single component that we call the “highly excited” component. It is probable that the strongest $J = 5$ lines show a weak wing that represents a small fraction of the absorption. However, our analysis primarily relies upon the weakest $J = 5$ lines. As a predictive guide to the vibrationally excited lines, we estimated the strength of each putative line based on column densities toward HD 37903 derived from a high resolution *HST* STIS spectrum (Meyer et al. 2002) which shows similar H₂ excitation to our spectrum of Herschel 36. We then selected lines from the Abgrall et al. (1993a,b) lists that were most likely to be unblended and visible at the lower resolution and sensitivity of the *FUSE* spectra.

Given that the observed excited H₂ line profiles are dominated by the *FUSE* instrumental profile, which is reasonably modeled by a Gaussian especially at low to moderate S/N (e.g., Jensen et al. 2010), we measured lines by fitting Gaussian profiles. Thus, we obtained central wavelength, line depth, and line width, the latter two quantities directly give the equivalent width of the line and a formal uncertainty. We combined this uncertainty in quadrature with a continuum uncertainty estimated from the line width and the noise in the continuum fit. In many cases, this likely overestimates the true uncertainties. However, continuum placement is a particular challenge here given the likelihood of otherwise undetected vibrationally excited lines contaminating the continuum, analogous to the “line fog” seen in optical spectra of late-type stars. When possible, adjacent H₂ lines were deblended with multiple Gaussians.

Although our technique was to measure lines and perform a curve-of-growth analysis, there is significant line confusion due to the wealth of detectable transitions, most of which have never been observed in *FUSE* spectra. Thus, we followed an iterative process whereby we generated a model spectrum from the curve-of-growth analysis, used that to check if the levels were reasonably modeled, and then explored individual lines again. Many lines were eliminated based on the modeling suggesting that a stronger line may be contaminated by a weaker line. This procedure leverages the strength of the curve-of-growth method (i.e., deriving the b -value and column densities simultaneously with the cleanest lines) while not having to fully model the continuum, stellar flux, and instrumental function across the entire spectrum.

Despite the first observation having a longer exposure time, the second observation was of higher quality and we were able to measure more lines. Thus we used the second observation as the primary source for the excited

² Throughout this paper we will apply the usual convention of writing the lower rotational level of an absorption transition, J'' , as simply J , and similarly writing the lower vibrational level as v .

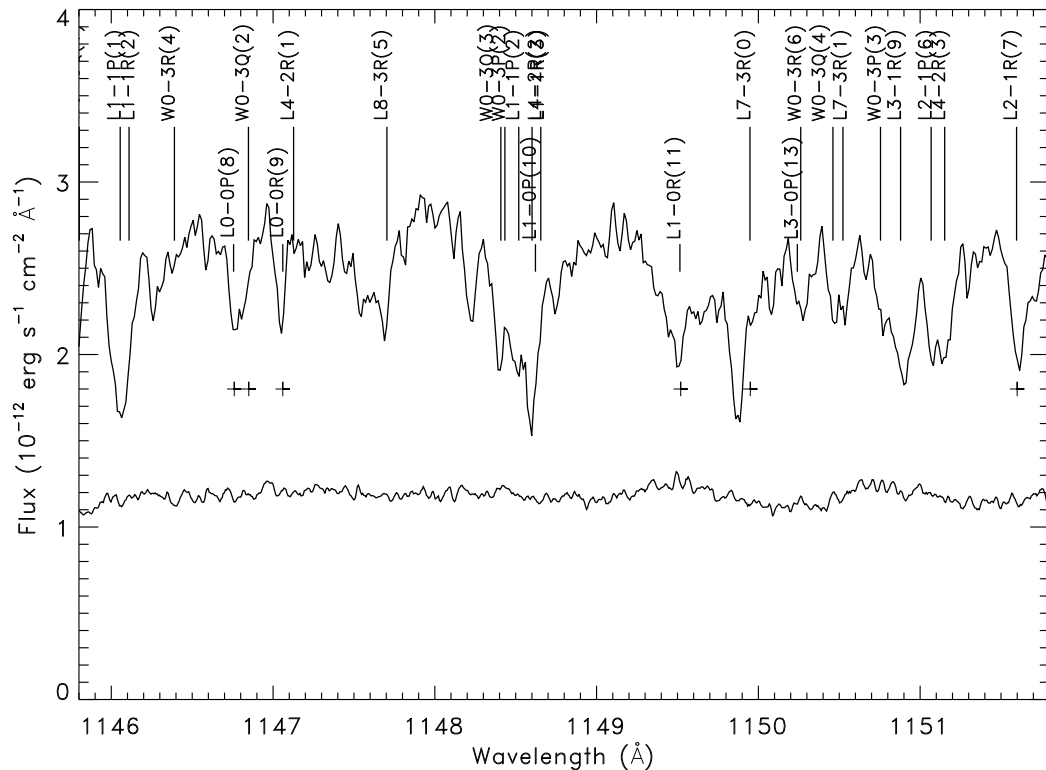


FIG. 1.— A portion of the second observation showing numerous lines from vibrationally excited states (upper row of labels and long tick marks), and high-excitation states of the vibrational ground state. The lower rotational level of the transition (J) is given in parentheses and the lower vibrational level (v) is given before the branch label (P , Q , or R). The *FUSE* spectrum of M8 star HD 164906 is shown for comparison, with the continuum normalized to about half of the Herschel 36 continuum. The lack of ISM features in this portion of the spectrum is the overwhelmingly typical case in *FUSE* spectra. Weak line identifications for the Herschel 36 spectrum are generally not included, nor are atomic lines. Lines specifically used in later analysis are indicated directly below the line.

lines. Unfortunately, even in the second observation most lines were detected below the $3\text{-}\sigma$ level relative to the combined measurement uncertainties and continuum uncertainties.

Our final list included 122 lines from 37 ro-vibrational levels in the second observation, and we successfully measured 72 of those lines in the first observation. Figure 2 shows that there is reasonable agreement in the equivalent widths of these lines, albeit with large uncertainties. This indicates that there was not a dramatic change in the strength of the excited component between the two observations, and allows us to treat the second observation as representative. We note that absorption from additional ro-vibrational levels is evident in the second spectrum, but we limited the analysis to levels where we were most confident that at least one uncontaminated line could be decisively measured.

We performed least squares fits of the equivalent widths from the second observation to a grid of single-component curves of growth with 0.1 km s^{-1} spacing in b . We attempted fits for lines from various combinations of ro-vibrational states and consistently found small b -values less than 2 km s^{-1} for most of these combinations. Thus, we adopted the overall best-fit of $b = 1.2 \text{ km s}^{-1}$. In Figure 3, we show the $J = 5\text{--}9$ levels of the vibrational ground state, which carry most of the weight in the curve of growth fits. The resulting column densities for all measured levels are given in Table 2.

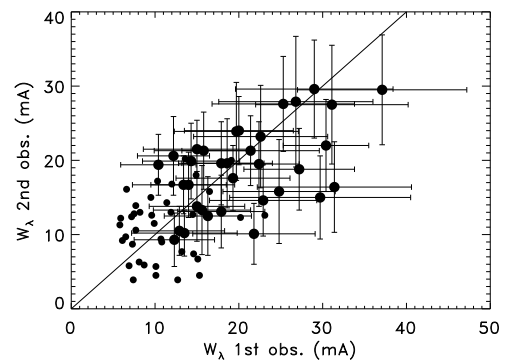


FIG. 2.— Equivalent width comparison between observations. Lines detected at above the 2-sigma level are shown with error bars and larger symbols. Solid line: unit slope passing through zero.

Our b -value and column densities are rather poorly constrained due to the large relative errors on most individual lines. Based on the curve-of-growth analysis for the measured lines, the 1σ error range for the b -value is $0.1\text{--}4.1 \text{ km s}^{-1}$. However, we have the additional constraint of modeling the spectra which allows us to look at blended lines and undetected lines in addition to the relatively small fraction of isolated lines. Thus, we are more confident in the derived b -value than would be warranted by purely the analysis of measured lines.

TABLE 2
LOGARITHMIC H₂ COLUMN DENSITIES FOR THE HIGHLY EXCITED MATERIAL, 2ND OBSERVATION^a

| J | $N(v=0)$ | $N(v=1)$ | $N(v=2)$ | $N(v=3)$ | $N(v=4)$ |
|-----|------------------------------|-----------------------------|-----------------------------|-----------------------------|-----------------------------|
| 0 | | $14.54^{+0.78}_{-0.57}$ (4) | $13.49^{+3.75}_{-1.30}$ (2) | $13.71^{+4.66}_{-1.74}$ (1) | $13.88^{+1.01}_{-0.67}$ (2) |
| 1 | | $14.25^{+1.28}_{-0.59}$ (3) | $14.17^{+1.31}_{-0.62}$ (3) | $13.74^{+0.72}_{-0.36}$ (3) | $13.38^{+1.03}_{-0.47}$ (2) |
| 2 | | $15.22^{+2.09}_{-0.94}$ (2) | $14.04^{+1.35}_{-0.62}$ (1) | $13.84^{+1.22}_{-0.49}$ (3) | $13.33^{+0.54}_{-0.32}$ (2) |
| 3 | | $15.26^{+0.87}_{-0.87}$ (9) | $14.36^{+1.57}_{-0.62}$ (1) | $14.19^{+2.55}_{-1.20}$ (3) | $13.93^{+1.63}_{-0.62}$ (1) |
| 4 | | $15.16^{+0.80}_{-0.81}$ (5) | $14.14^{+1.16}_{-0.53}$ (2) | $14.45^{+1.72}_{-0.65}$ (5) | |
| 5 | $16.66^{+0.53}_{-0.72}$ (3) | $14.73^{+1.10}_{-0.71}$ (6) | $13.87^{+0.93}_{-0.41}$ (1) | $13.45^{+0.78}_{-0.42}$ (2) | |
| 6 | $15.71^{+0.97}_{-0.81}$ (3) | $14.32^{+1.73}_{-0.67}$ (4) | | | |
| 7 | $16.08^{+0.70}_{-0.66}$ (5) | $15.13^{+0.99}_{-0.94}$ (4) | $14.25^{+1.54}_{-0.57}$ (1) | $13.55^{+1.31}_{-0.50}$ (2) | |
| 8 | $15.70^{+0.80}_{-0.87}$ (6) | | $13.51^{+0.56}_{-0.34}$ (1) | | |
| 9 | $15.74^{+0.93}_{-0.74}$ (11) | | | $13.69^{+1.07}_{-0.47}$ (2) | |
| 10 | $15.05^{+1.33}_{-0.73}$ (5) | | | | |
| 11 | $14.93^{+1.09}_{-0.59}$ (5) | | | | |
| 12 | $14.19^{+2.12}_{-0.71}$ (2) | | | | |
| 13 | $14.48^{+1.54}_{-0.61}$ (5) | | | | |

^a The number in parentheses behind the column density is the number of lines measured in that level.

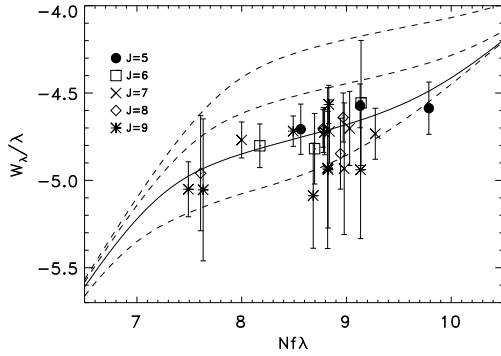


FIG. 3.— Best-fit curve of growth ($b=1.2$ km s⁻¹) for second observation, with lines from the $J = 5-9$ levels from the ground vibrational state, which provide most of the weight in the fit. Curves of growth for $b = 2.4$ and 4.8 km s⁻¹ are shown above the best fit, and $b = 0.6$ km s⁻¹ is shown below.

The derived b -value for the highly excited H₂ is quite small; we are unaware of any smaller values ever found in absorption. Other lines of sight with considerable vibrational excitation have also shown relatively small b -values with a single component even at a resolution of ~ 3 km s⁻¹ from *HST* data (Meyer et al. 2001 and Gnaciński 2011 for HD 37903 from *FUSE* and *HST*; Boissé et al 2005 for HD 34078 from *FUSE*; Gnaciński 2013 for HD 147888 *FUSE* and *HST*). Smaller b -values of less than 1 km s⁻¹ are seen for individual components of various atomic species in many lines of sight in spectra with ~ 1 km s⁻¹ resolution (e.g., Welty & Hobbs 2001). However, due to the lack of ultra high resolution UV observations, we do not know if this holds for H₂ as well, and the low mass of the molecule also works against very small b -values. For purely thermal broadening, $b_{\text{H}_2} = 1.2$ km s⁻¹ corresponds to a temperature of 174 K. This should be contrasted with the E/k values for the $v = 1$ rotational levels which are $\gtrsim 6000$ K, rising to $\gtrsim 22000$ K for $v = 4$, indicating that the observed excitation is due to a non-thermal process.

To further assess the excitation, in Figure 4, we present an excitation diagram based on the column densities in

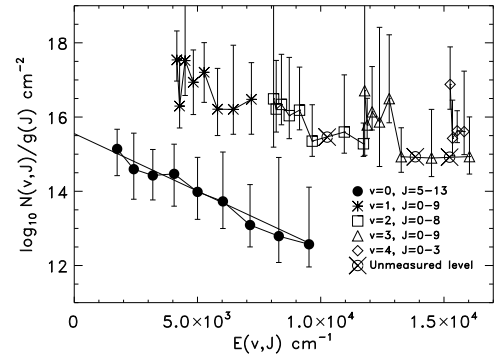


FIG. 4.— Excitation diagram for the second observation of Herschel 36. The excited vibrational levels have each been shifted upward by three dex relative to the $v = 0$ level for clarity. Unmeasured levels are labeled for clarity at the interpolated location between adjacent levels. The Boltzmann excitation fit for $J = 5-9$ of the $v = 0$ level is shown, and extrapolated to cover $J = 0-13$.

Table 2. The large uncertainties are particularly apparent here, but the expected decreasing trend with increasing J of the quantity column density divided by statistical weight is generally seen. The uncertainties make a more detailed quantitative modeling analysis difficult, as a broad range of cloud models could fit the column densities within the large uncertainties. However, a comparison with the apparently similar and better constrained situation with HD 37903 may be instructive.

HD 37903 was analyzed by Meyer et al. (2001) using only the high-quality *STIS* data, and has been recently re-analyzed by also including *FUSE* data which provided column densities for non-vibrationally excited levels (Gnaciński 2011). In both analyses, interstellar cloud models favored an interpretation whereby the extreme H₂ excitation was occurring in a relatively dense cloud of material ~ 0.5 pc away from HD 37903.

In Figure 5, we plot the excitation diagram for Herschel 36, along with those for HD 37903 (Gnaciński 2011) and HD 34078 (Boissé et al 2005). These are the two lines of sight that show the strongest vibrationally excited lines, although HD 34078 only has column densities for relatively few highly excited levels. Again, our values are

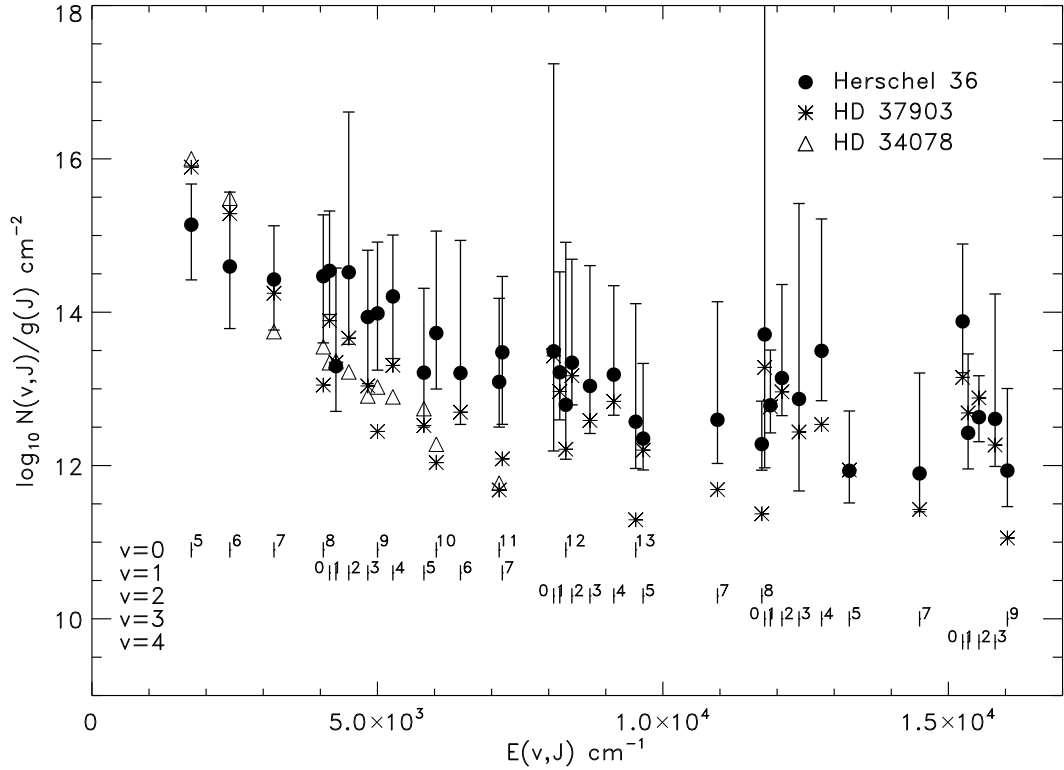


FIG. 5.— Excitation diagram comparison for Herschel 36, HD 37903, and HD 34078. Level identifications are given at the bottom of the plot with v at the left, and J near the appropriate tick mark.

highly uncertain, but the three lines of sight all show relatively large amounts of excited material, with evidence that the Herschel 36 column densities are even larger than those towards the other two stars. These lines of sight should be contrasted with the finding of Jensen et al. (2010) of 3σ upper limits of $\lesssim 10^{13} \text{ cm}^{-2}$ for the $v = 1$, $J = 0$ level for nearly all *FUSE* translucent lines of sight as compared with our logarithmic column density of 14.54 for Herschel 36, 13.89 for HD 37903, and 13.34 for HD 34078. This means that vibrationally excited column densities for most lines of sight would be well below those seen in Figure 5. The few other lines of sight where vibrationally excited H₂ has been detected in absorption also show smaller column densities those in Figure 5; i.e., Federman et al. (1995) for ζ Oph, Jensen et al. (2010) for HD 38087 and HD 199579, and Gnaniński (2013) for HD 147888. In none of the cases has velocity structure been seen within vibrationally excited lines, even in *HST* data with 3 km s^{-1} resolution.

For a different perspective, in Figure 6, we plot the column densities of the excited levels relative to the total line-of-sight H₂ column densities. Since the total H₂ column density towards Herschel 36 is smaller than for the other two lines of sight, the differences are exaggerated. However, in reality, the differences may be even greater. As we discuss in § 3.3, much of the line-of-sight material toward Herschel 36 may lie in the foreground of M8 and not be directly related to the highly excited material near the star itself. Thus, the relative column densities of the highly excited levels may be even higher in the material that lies within M8 itself.

3.2. The highly excited component in the context of the line of sight material

Figures 7 and 8 reveal the difficulty in interpreting low-excitation states in the highly excited component. Broad structure appears for the $J = 2-4$ lines (we omit $J = 4$ because with the weaker lines, the structure is not as obvious), and the highly excited component does not match either of the apparent peaks of the $J = 2-3$ structure. Nor does the highly excited component appear to represent more than a small fraction of the observed velocity range of $J = 2-3$. If the highly excited component were to actually represent either of the $J = 2-3$ peaks or the bulk of the $J = 0-1$ profiles, it would require an unrealistic velocity shift of more than 20 km s^{-1} between $J = 5$ and the lower levels.

In modeling the spectrum of the highly excited component for a variety of ro-vibrational bandheads and thus a range of oscillator strengths, we find that $J = 0-1$ logarithmic column densities $\gtrsim 18.5$ clearly “overshoot” the observed profiles at those wavelengths. These values are much smaller than the total line of sight values reported by Rachford (2009); 19.92 and 19.86, respectively.

We can set an uncertain *lower* limit on the low- J column densities of the highly excited material by using the excitation diagram in Figure 4. If we fit a line to the $J = 5-10$ levels of the ground vibrational state, we obtain a Boltzmann excitation temperature of $2019^{+5675}_{-875} \text{ K}$ (a fit of $J = 5-8$ gives a similar result). If we extrapolate this line to lower levels, we obtain logarithmic column densities of 15.48, 16.40, 16.08, 16.60, 16.10, for $J = 0, 1, 2, 3$, and 4, respectively. While the column densities

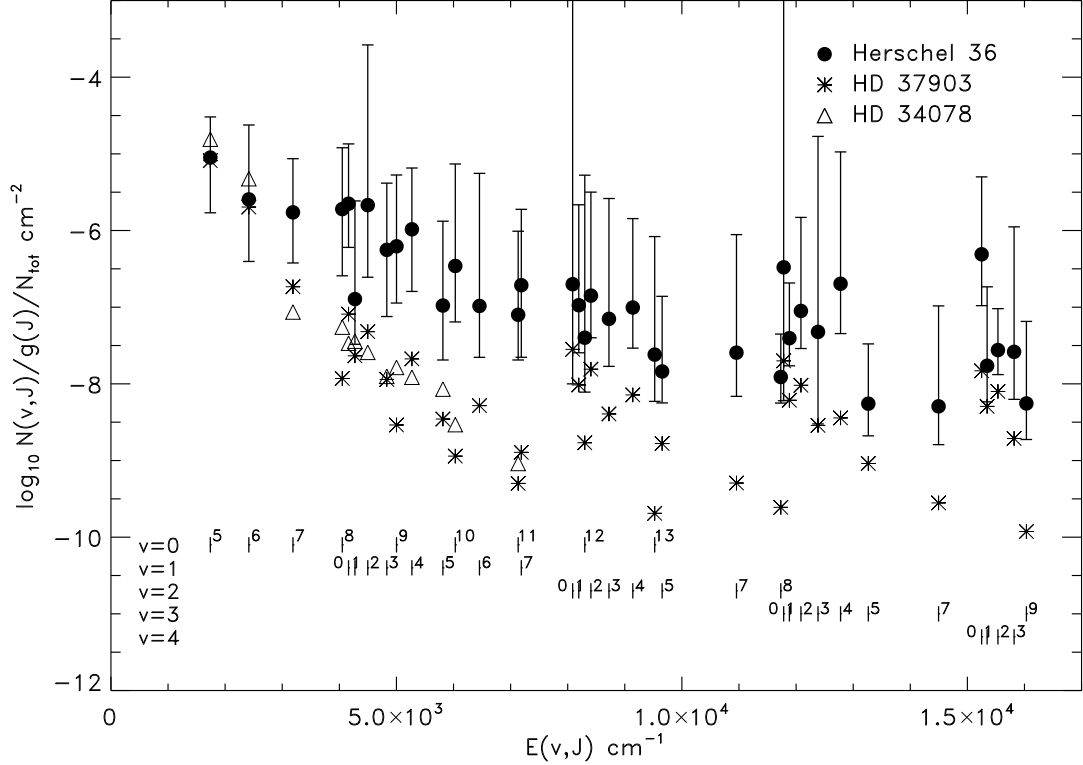


FIG. 6.— Excitation diagram comparison for Herschel 36, HD 37903, and HD 34078, normalized to the total H_2 column density for the line of sight. Otherwise the same as Fig. 5.

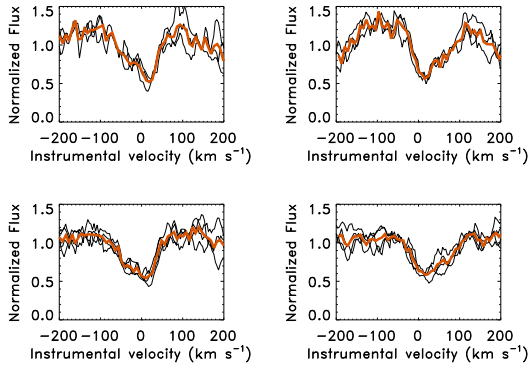


FIG. 7.— Broad velocity structure in several $J = 2$ and $J = 3$ lines in the first and second observations. Upper left: $J = 2$, first observation; Upper right: $J = 2$, second observation; Lower left: $J = 3$, first observation; Lower right: $J = 3$, second observation. Three lines of similar strength are shown for $J = 2$, and four lines are shown for $J = 3$. The thick lines are averages.

for $J = 0$ and $J = 1$ may be significantly underestimated by this fit, it is common for $J = 2$ or 3 to 6 and beyond to be reasonably fit by a single line (see, e.g., Jensen et al. 2010). Unless we dramatically increase the b -values, column densities much greater than these for $J = 2$ –4 will “overshoot” the observed profiles. The evidence for b -value changes as a function of J (e.g. Jenkins & Pembert 1997; Lacour et al. 2005) is that the more highly excited levels that may show larger b -values, a trend we do not see in our data. Significantly smaller column densities are not physically compatible with the levels that we have been able to measure; i.e., they would not follow

a Boltzmann equilibrium trend.

Based on the arguments in the previous two paragraphs, our best estimates of the logarithmic column densities of the $J = 0$ –4 levels of the highly excited component are $\lesssim 18.0$, $\lesssim 18.0$, 16.1, 16.6, and 16.1, respectively. While the material responsible for the extended velocity structure may lie within M8, it does not produce measurable absorption in the more highly excited levels above $J = 5$, and thus must be much further from a strong UV source, and/or strongly shielded from UV radiation.

The final difficulty in interpreting the highly excited component is a significant velocity shift during the 3.4 year gap between observations. Figure 9 shows both observations with the wavelength solutions given by the CALFUSE 3.2.1 pipeline. For clarity, only lines from the vibrational ground state have been labeled; recall that levels $J \geq 5$ are part of the highly excited material that shows no component structure. The line labels have not been shifted in this plot, and they line up to within several km s^{-1} of the appropriate lines in the spectrum, as do the excited lines themselves. However, the $J = 0$ –1 bandhead is clearly offset between the two observations. In contrast, as shown in Figure 10, if we shift the second observation redward by 60 km s^{-1} , the $J = 0$ –1 bandheads line up, while the excited material does not.

We note that the difference in the total of the geocentric and heliocentric corrections for the two observations is 53 km s^{-1} ; we first looked at this data before heliocentric corrections were implemented in CALFUSE, which resulted in a “raw” plot that looked like Figure 10 rather than Figure 9. However, it seems highly unlikely that the bulk of the material – which appears to be in the

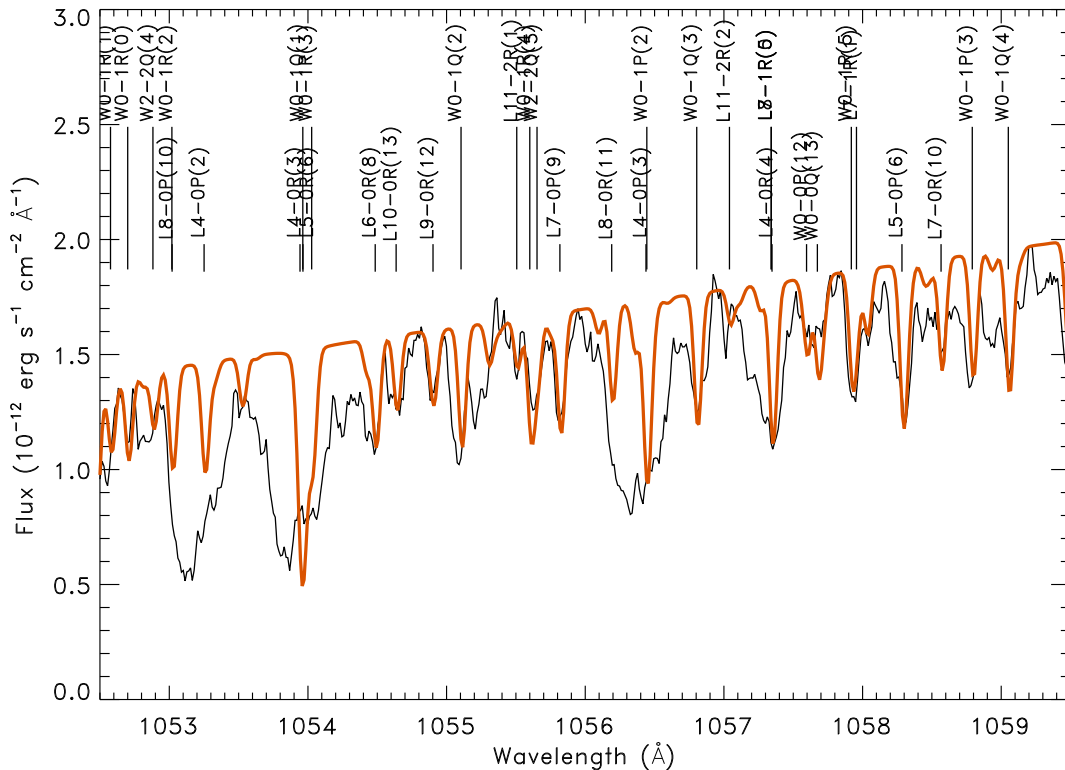


FIG. 8.— Model of the highly excited component compared with second observation. Note that the model continuum is only approximate. Atomic lines (e.g., Fe II $\lambda 1055$) have not been modeled and the $J = 2-4$ column densities for the highly excited component have been estimated using the excitation diagram in Figure 4 as described in the text. For clarity, only the strongest vibrationally excited lines are labeled.

foreground of M8 – has undergone such a large velocity shift. Thus, a ~ 60 km s $^{-1}$ redshift must have occurred in the highly excited material relative to the bulk of the material. This also indicates a ~ 60 km s $^{-1}$ deviation in the wavelength scale that was applied to the two observations, even though it appears that the correct geocentric and heliocentric corrections were applied. Systematic velocity errors in Version 3 of CALFUSE can be 10 km s $^{-1}$ or more (Dixon et al 2007) in certain circumstances.

Both *FUSE* observations of Herschel 36 were made through the 30'' square LWRs aperture. As noted by Boissé et al. (2009), in comparing *FUSE* observations of HD 34078 taken through the LWRs aperture with an observation taken with the 4'' \times 20'' MDRS aperture, there were subtle H $_2$ line profile/strength differences. They attributed these differences to the extra diffuse nebular emission passing through the factor of 900/80 larger aperture. Based on extinction curves from Fitzpatrick & Massa (2007), the total extinction at 1100 Å toward Herschel 36 is 8.5 mag as compared to 6.4 mag for HD 34078, so we might expect scattered light to be a bigger issue for Herschel 36. Some combination of excess diffuse emission, variations in the position of the LWRs on the sky, and variations in the path of light through the cloud from the 3 au orbit in the triple system may conspire to produce changes in the appearance of the two spectra of Herschel 36. However, such an effect would have to produce the very specific large velocity shift of the highly excited lines without large variations in the strength or width of the lines, and simultaneously the large profile

variation specifically seen in the $J = 2-4$ lines. Nothing like this is seen toward HD 34078, or any other *FUSE* observations of which we are aware.

We are unaware of any additional strong point-like UV sources within 30'' of the Herschel 36 system that are visible from Earth and thus might produce a composite spectrum. We also note that in modeling the $J = 0-1$ lines, adding a shifted component even with $\sim 1\%$ of the total material caused the modeled profile to deviate strongly from the observed absorption.

3.3. Comparison with H $_2$ along other lines of sight toward M8

Herschel 36 shows considerably more reddening than most stars in the M8 complex (McCall et al. 1990). Three stars with $E(B - V) = 0.30-0.45$ have been observed in the far UV at moderate-to-high resolution along lines of sight within ~ 10 arcminutes of Herschel 36, and all are apparently associated with M8 (McCall et al. 1990). Dahlstrom et al. (2013) give considerably more detail on this portion of M8; here we provide the first published analysis of H $_2$ towards three stars relatively near Herschel 36.

HD 164794 (9 Sgr) lies 3 arcminutes from Herschel 36 (1.3 pc at 1.5 kpc), and was observed with *ORFEUS* in 1993. Unfortunately, the velocity resolution was only ~ 90 km s $^{-1}$, insufficient to see even a broad velocity structure in H $_2$ such as that toward Herschel 36. HD 164816 (5.5 arcmin from Her 36) and HD 164906 (10.4 arcmin), have both been observed with *FUSE* at the same

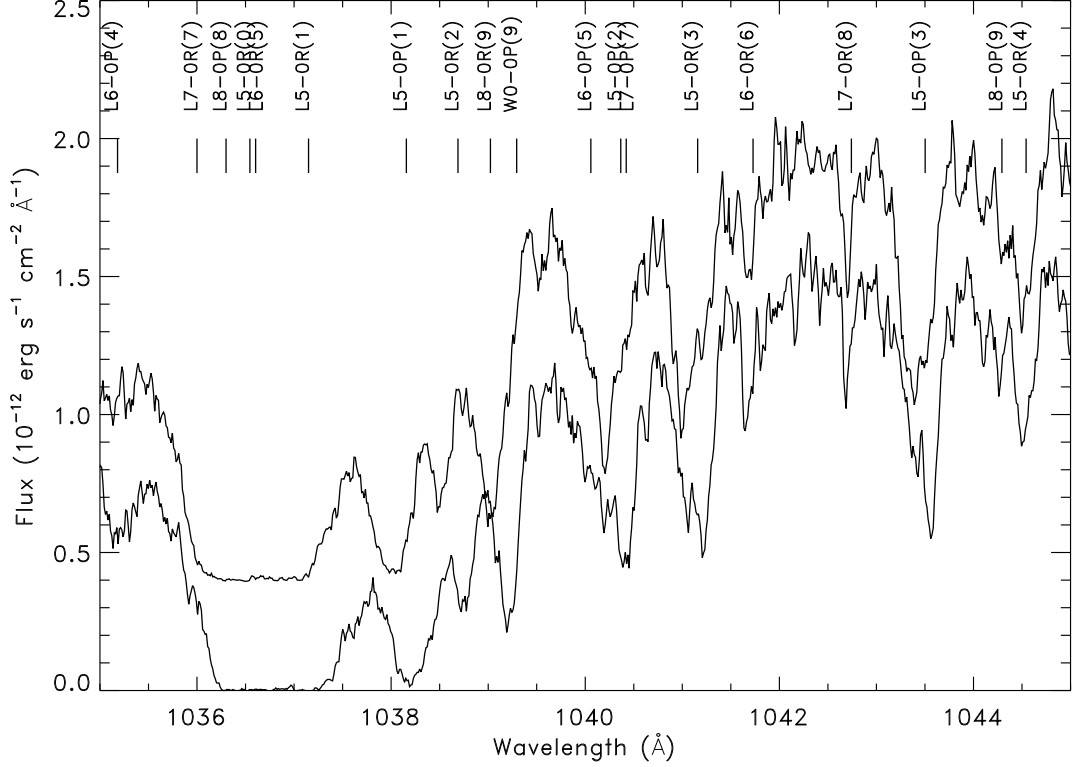


FIG. 9.— Portion of both Herschel 36 observations; the second observation has been shifted upward. Note that the highly excited H_2 lines line up. The strong feature in both spectra between 1039 Å and 1039.5 Å is due to O I.

TABLE 3
LOGARITHMIC H_2 COLUMN DENSITIES FOR HERSCHEL 36 AND NEARBY LINES OF SIGHT

| Star | Ang. sep. (') | Dist. ^a (pc) | E(B-V) | $N(H_2)$ | $N(J=0)$ | $N(J=1)$ | $N(J=2)$ | $N(J=3)$ | $N(J=4)$ | $N(J=5)$ |
|-------------|------------------|----------------------------|--------|----------|----------|----------|----------|----------|----------|----------|
| Herschel 36 | 0.00 | 0.0 | 0.87 | 20.19 | 19.92 | 19.86 | | | | 16.66 |
| 9 Sgr | 2.95 | 1.3 | 0.35 | 20.10 | 19.85 | 19.73 | 16.60 | | | |
| HD 164816 | 5.48 | 2.4 | 0.30 | 20.03 | 19.76 | 19.69 | 16.86 | 15.84 | 14.76 | 14.51 |
| HD 164906 | 10.36 | 4.5 | 0.45 | 20.23 | 19.96 | 19.89 | 16.90 | 15.89 | 14.76 | 14.29 |

^a Linear plane-of-sky separation assuming stellar distance of 1500 pc.

resolution as the Herschel 36 observation.

The low resolution of *ORFEUS* limits our analysis of 9 Sgr to the $J = 0-2$ states, and even $N(2)$ is rather uncertain. However, for these states there is excellent agreement between 9 Sgr and HD 164816, as can be seen in Table 3. HD 164906 is much farther from Herschel 36, but the column densities are still only somewhat larger than for the other lines of sight. Importantly, neither of the *FUSE* observations show any hint of the highly excited material seen towards Herschel 36, nor the broad $J = 2-4$ component structure, as clearly seen in Figure 11.

The actual H_2 column densities observed toward the stars in M8 are all relatively small given the amount of extinction, i.e., $f_{H_2} \lesssim 0.1$, but particularly for Herschel 36. In fact, $N(H_2)$ is only slightly larger toward Herschel 36 than the other lines of sight despite having twice the reddening. All of the stars have among the smallest molecular fractions for Galactic lines of sight with $A_V > 1$ (e.g. Rachford et al. 2002, 2009), and Herschel 36 is the

smallest of which we are aware. The key point is that the parameters of the bulk of the molecular material in front of a large portion of M8 are relatively uniform and there is no evidence of unusually strong excitation, except in the Herschel 36 observation. Thus, the evidence points towards the highly excited material near Herschel 36 representing the portion of the total line of sight material that lies in a cloud (or clouds) near the star system.

3.4. Molecular hydrogen and carbon monoxide emission in the vicinity of Herschel 36

Emission from vibrationally excited H_2 has been seen near Herschel 36 (Burton 2002). The $2.12 \mu m$ $1-0 S(1)$ transition was detected from a roughly bipolar shape centered on Herschel 36, with a peak flux corresponding to a $v = 1, J = 3$ column density of $1.4 \times 10^{16} \text{ cm}^{-2}$ uncorrected for extinction. Even without the correction for the IR extinction, this is still much greater than our derived column density for this level of $1.8 \times 10^{15} \text{ cm}^{-2}$. In fact, Burton (2002) observed that this peak emission

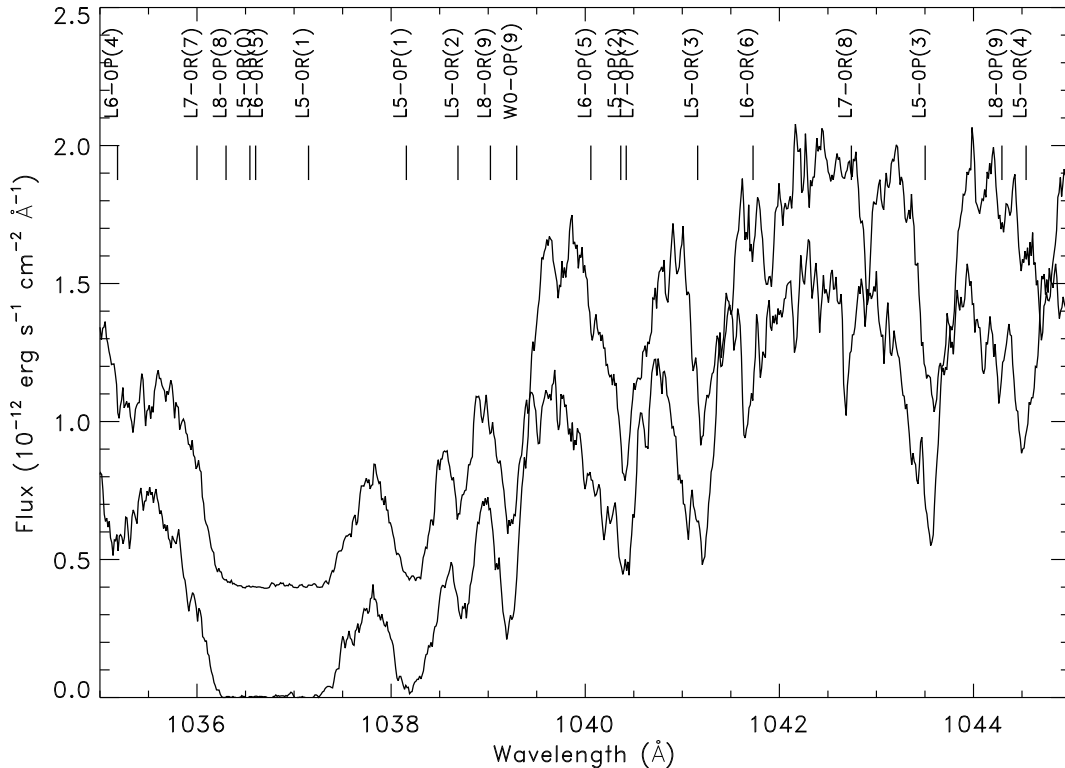


FIG. 10.— Portion of both Herschel 36 observations; the second observation has been shifted upward and shifted redward by 60 km s^{-1} to line up the H_2 $J = 0-1$ bandheads. The strong feature at 1039.2 Å is due to O I.

occurs nearly 2 arcsec from Herschel 36. Given the projection of the bipolar structure on either side of Herschel 36 in the plane of the sky, little of this material may be directly in front of the star system. Thus, the conclusion by Burton (2002) that the H_2 emission was tracing shock-heated gas does not mean that the highly excited H_2 we see along the narrow beam to the stars in the Herschel 36 system is the same material.

Similarly, the region around Herschel 36 contains one of the strongest known CO emission sites (White et al. 1997). They estimated a peak column density of $2.1 \times 10^{16} \text{ cm}^{-2}$ for $\text{N}(\text{C}^{18}\text{O})$ alone. The CO peak was located very near the star, but the beamwidths were 11–22 arcsec, depending on the observed transition. Since our observed $\text{N}(\text{H}_2)$ appears to be much smaller than that implied by the peak CO emission, it is not surprising that the CO abundance observed in absorption toward Herschel 36 is quite small. Although it is hard to precisely measure the extent of the weak rotationally excited lines on either side of the $J = 0$ line due to S/N issues, the E–X 0–0 band at 1076 Å implies $N(\text{CO}) \lesssim 10^{14} \text{ cm}^{-2}$, or a CO/ H_2 ratio of $\lesssim 6 \times 10^{-7}$, consistent with direct UV pencil-beam derived ratios along lines of sight with similar abundances (Burgh, et al. 2007, Sonnentrucker et al. 2007, Sheffer et al. 2008). Clearly, both H_2 and CO show considerable spatial variability in the plane of the sky, and/or there is considerable material behind Herschel 36. This is consistent with the complex environment of Herschel 36 summarized by Dahlstrom et al. (2013).

4. CONCLUSIONS AND FUTURE DIRECTIONS

The region near Herschel 36 is very complex and has been studied at a variety of wavelengths. Our far-UV observations provide the first look at H_2 along the line of sight towards the UV-bright Herschel 36 star system.

We have found an absorption component displaying highly excited H_2 apparently lying near the Herschel 36 system which is subjected to an intense radiation field and experienced a $\sim 60 \text{ km s}^{-1}$ redshift during a 3.6-year period. This component does not appear to be at the same velocity as the material which dominates the lower excitation, and this latter material does not appear to produce visible absorption beyond $J = 5$. Given the width of the $J = 2-3$ lines in the spectrum, multiple additional components may exist and/or there may be material in a relative narrow physical distance range but spread across a large velocity range. The highly excited component – the primary focus of this paper – appears to only contain a small fraction of the total H_2 along the line of sight on the order of 1%.

While certain portions of the material surrounding the Herschel 36 system may be associated with outflows or jets and thus be shock heated (Burton 2002), the material in the immediate foreground seen in our observations appears similar to that seen in front of HD 37903 which has been interpreted as the result of fluorescent excitation due to the strong UV field near the stars (Meyer et al. 2001; Gnaniński 2011).

Other unusual excitation has been seen toward the Herschel 36 system. Dahlstrom et al. (2013) reported the first known detection of rotationally excited CH and

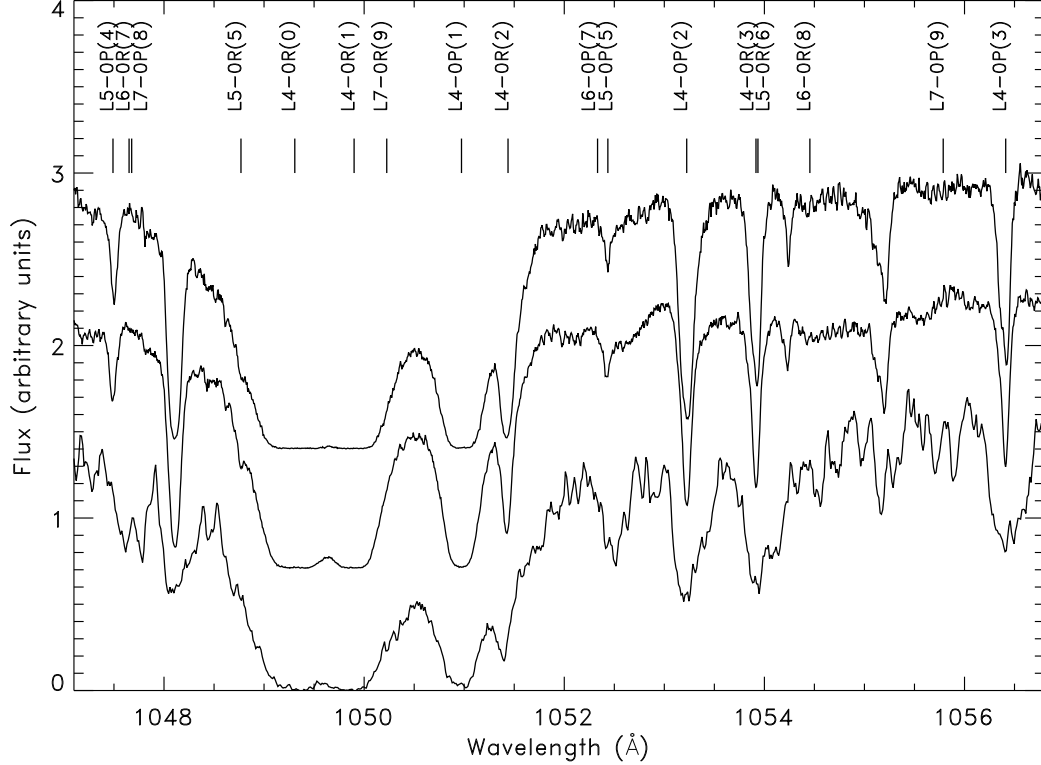


FIG. 11.— From top to bottom; HD 164906, HD 164816, Herschel 36 second observation. The former spectra were normalized to roughly match the flux of the Herschel 36 observations before being shifted upward. The line identifications are matched to the wavelength scale of the two HD stars, and would be slightly redshifted to match Herschel 36. Note the lack of velocity structure in the $J = 2-4$ lines towards HD 164906 and HD 164816 and the lack of highly excited material. The strong features at 1048 Å and 1055 Å are due to Ar I and Fe II, respectively.

CH^+ in absorption. This excitation is attributed by Oka et al. (2013) to far-IR radiation from a source ~ 375 au from the main stellar triplet, believed to be a heavily embedded B-type star (Goto et al. 2006). Unusual redward wings have been seen in some Diffuse Interstellar Bands (DIBs) toward Herschel 36, again thought to trace high levels of rotational excitation of the molecule(s) responsible for the DIBs (Dahlstrom et al. 2013). The environment near the Herschel 36 system is thus an important laboratory for studying the effects of the intense radiation fields in young star clusters on gas and dust.

HST observations with *STIS* would provide a wealth of additional information on Herschel 36. First, we could much more precisely study the highly excited H_2 via the hundreds of ro-vibrational transitions available longward of 1150 Å. This would permit precise enough column densities for a detailed modeling analysis of the excitation. Second, the same observations will provide high

resolution observations of numerous atomic and molecular species. This will allow us to assess the true velocity structure down to 3 km s^{-1} resolution, and potential information on the physical conditions in the various components.

This work is based on data obtained for the Guaranteed Time Team by the NASA-CNES-CSA *FUSE* mission operated by the Johns Hopkins University. This research has made use of the SIMBAD database, operated at CDS, Strasbourg, France. We wish to thank D. York, D. Welty, L. Hobbs, and the anonymous referee for helpful comments. BLR would like to thank the University of Colorado's Center for Astrophysics and Space Astronomy for use of facilities during a sabbatical leave when much of this work was completed. Partial support for this work has been provided by the National Science Foundation, under grant AST-1008801 (BLR).

Facilities: FUSE, ORFEUS

REFERENCES

- Abgrall, H., Roueff, E., Launay, F., Roncin, J.-Y., & Subtil, J.-L. 1993a, *A&AS*, 101, 273
- Abgrall, H., Roueff, E., Launay, F., Roncin, J.-Y., & Subtil, J.-L. 1993b, *A&AS*, 101, 323
- Arias, J. I. et al. 2010, *ApJ*, 710, L30
- Boissé, P., Le Petit, F., Rollinde, E., Roueff, E., Pineau des Forêts, G., Andersson, B.-G., Gry, C., Felenbok, P. 2005, *A&A*, 429, 509
- Boissé, P., Rollinde, E., Hily-Blant, P., Pety, J., Federman, S. R., Sheffer, Y., Pineau des Forêts, G., Roueff, E., Andersson, B.-G., Hébrard, G. 2009, *A&A*, 501, 221
- Burgh, E. B., France, K., & McCandliss, S. R. 2007, *ApJ*, 658, 446
- Burton, M. G. 2002, *PASA*, 19, 260
- Cannon, A. J. & Pickering, E. C. 1922, *Ann. Harv. Coll. Obs.*, 97, 1
- Dahlstrom, J. et al. 2013, *ApJ*, 773, 41
- Dixon, W. V. et al. 2007, *PASP*, 119, 527

- Federman, S. R., Cardell, J. A. van Dishoeck, E. F., Lambert, D. L., & Black, J. H. 1995, *ApJ*, 445, 325
- Fitzpatrick, E. L. & Massa, D. 2007, *ApJ*, 663, 320
- Goto, M., Stecklum, B., Linz, H., Feldt, M., Henning, T., Pascucci, I., & Usuda, T. 2006, *ApJ*, 649, 299
- Gnaciński, P. 2011, *A&A*, 532, A122
- Gnaciński, P. 2013, *A&A*, 549, 37
- Hecht, J., Helfer, H. L., Wolf, J., Donn, B., & Pipher, J. L. 1982, *ApJL*, 263, 39
- Herschel, J. F. W. 1847, Results of astronomical observations made during the years 1834, 5, 6, 7, 8 at the Cape of Good Hope (London: Smith, Elder, and Co.), pg. 16
- Jensen, A. G., Snow, T. P., Sonneborn, G., & Rachford, B. L. 2010, *ApJ*, 711, 1236
- Jenkins, E. B. & Peimbert, A. 1997, *ApJ*, 477, 265
- Lacour, S., Ziskin, V., Hébrard, G., Olivier, C., André, M. K., Ferlet, R., & Vidal-Madjar, A. 2005, *ApJ*, 627, 251
- McCall, M. L., Richer, M. G., & Visvanathan, N. 1990, *ApJ*, 357, 502
- Meyer, D. M., Lauroesch, J. T., Sofia, U. J., Draine, B. T., Bertoldi, F. 2001, *ApJL*, 553, 59
- Moos, H. W. et al. 2000, *ApJ*, 538, L1
- Oka, T., Welty, D. E., Johnson, S., York, D. G., Dahlstrom, J., Hobbs, L. M. 2013, *ApJ*, 773, 42
- Rachford, B. L. et al. 2002, *ApJ*, 577, 221
- Rachford, B. L. et al. 2009, *ApJS*, 180, 125
- Sheffer, Y., Rogers, M., Federman, S. R., Abel, N. P., Gredel, R., Lambert, D. L., Shaw, G. 2008, *ApJ*, 687, 1075
- Sonnentrucker, P., Welty, D. E., Thorburn, J. A., York, D. G. 2007, *ApJS*, 168, 58
- Thackeray, A. D. 1950, *MNRAS*, 110, 343
- Welsh, B. Y. 1983, *ApJ*, 204, 1203
- Welty, D. E. & Hobbs, L. M. 2001, *ApJS*, 133, 345
- White, G. J., Tothill, N. F. H., Matthews, H. E., McCutcheon, W. H., Hultgren, M., & McCaughrean, M. J. 1997, *A&A*, 323, 529
- Wolff, N. J. 1961, *PASP*, 73, 432